Carbohydrate Polymers 264 (2021) 118039

Contents lists available at ScienceDirect

Carbohydrate Polymers

journal homepage: www.elsevier.com/locate/carbpol

Carboxylated cellulose nanocrystals with chiral nematic property from cotton by dicarboxylic acid hydrolysis

Chunxiang Lin [a,b,c], Beiqiu Chen [a], Yushi Liu [a], Yiting Chen [b], Minghua Liu [a,*], J.Y Zhu [c,*]

[a] College of Environment & Resources, Fuzhou University, Fuzhou, 350108, China
[b] Fujian Provincial University Engineering Research Center of Green Materials and Chemical Engineering (Minjiang University), Fuzhou, 350108, China
[c] Forest Products Laboratory, U.S. Department of Agriculture, Forest Service, Madison, WI, 53726, USA

ARTICLE INFO

Keywords:
Cellulose nanocrystals
Dicarboxylic acid hydrolysis
Chiral nematic
Birefringence

ABSTRACT

Carboxylated cellulose nanocrystals (CNCs) were produced from cotton linter using a mixture of a dicarboxylic acid (maleic acid or succinic acid) and its corresponding anhydride with or without catalyst in acetic acid as solvent. The low solubilities of these dicarboxylic acids can ease chemical recovery and decrease environmental impact (especailly maleic acid is a U.S. FDA approved indirect food additive (21CFR175-177)) and capital costs compared with the conventional concentrated sulfuric acid hydrolysis for producing CNCs. The dicarboxylic-acid-produced CNCs (DC-CNCs) contained surface carboxyl groups of approximately 0.5 mmol/g, with ranges of dimensions of 50–150 nm in diameter and 50–700 nm in length. Birefringence was observed in the DC-CNC suspensions above critical concentrations. However, fingerprint texture was only observed in the DC-CNC suspensions produced with catalyst *p*-toluenesulfonic acid. Scanning electron microscopy images of the cross section of DC-CNC films revealed a periodic ordered multilayer structure. DC-CNCs were also produced using recycled dicarboxylic acids.

1. Introduction

Cellulose nanocrystals (CNCs), produced from abundant and renewable cellulose sources, have attracted significant interest for their biocompatibility and excellent physical, chemical, and optical properties (Giese, Blusch, Khan, & MacLachlan, 2015; Hu, Omer, Ouyang, & Yu, 2018; Kelly et al., 2013; Kumar, I Matari, & Han, 2020). Among these properties, the ability to form a chiral nematic liquid crystal phase in concentrated solutions has attracted considerable interest (Elazzouzi-Hafraoui, Putaux, & Heux, 2009; Revol et al., 1994). After evaporating the solvent, the liquid crystal phase can form a chiral nematic CNC film (Dumanli et al., 2014) with intriguing optical properties for potential applications in security papers, nematic liquid crystal materials, optical materials, and mirrorless lasing (Giese et al., 2015; Kelly et al., 2013).

The formation of chiral nematic phase is mainly due to the repulsive steric and electrostatic interparticle forces induced by the negatively charged surfaces of rod-like CNCs (Dong, Revol, & Gray, 1998). In the conventional concentrated sulfuric acid hydrolysis process, sulfate half-ester groups carrying a negative charge are formed at the cellulose C6 position on the CNC surface (Revol, Bradford, Giasson, Marchessault, & Gray, 1992). The difficulties in economic sulfuric acid recovery and low thermal stability of sulfuric acid CNCs (Chen, Zhu, Baez, Kitin, & Elder, 2016; Roman & Winter, 2004), as well as the strong corrosive nature of sulfuric acid, makes sulfuric acid CNC unsustainable and less desirable. Alternative methods, such as oxidative methods using ammonia persulfate oxidation (Leung et al., 2011) as well as oxalic-acid-catalyzed potassium permanganate oxidation (Zhou et al., 2018), have been applied to produce CNCs with carboxyl groups and negative surface charge. However, the chiral nematic properties of these CNCs along with the recovery of process chemicals have not been evaluated nor demonstrated. When 2,2,6,6-tetramethylpiperidine-1-oxyl (TEMPO)-mediated oxidation was applied to chemically modify concentrated sulfuric-acid-hydrolysis-produced CNCs (Azzam, Heux, & Jean, 2016), carboxyl groups were formed as additional charge groups other than the sulfate half-ester groups on the surface of the starting sulfuric-acid-hydrolysis-produced CNCs, which enhanced the electrostatic interactions between CNCs to result in decreasing critical concentration of the CNC suspension for forming chiral nematic phase. A recent study, using CNCs produced by adding acrylic acid in sulfuric acid hydrolysis to form carboxyl as well as sulfate half-ester groups, also indicated that the chiral nematic phase properties are strongly

* Corresponding authors.
E-mail addresses: mhliu2000@fzu.edu.cn (M. Liu), junyong.zhu@usda.gov (J.Y Zhu).

https://doi.org/10.1016/j.carbpol.2021.118039
Received 31 January 2021; Received in revised form 31 March 2021; Accepted 3 April 2021
Available online 6 April 2021
0144-8617/Published by Elsevier Ltd.

dependent on the type and strength of the interaction force between CNCs (Cheng et al., 2019). Therefore, exploring sustainable CNC production methods that result in different surface charge groups other than conventional sulfate half-ester groups, along with understanding the impact of different surface charge groups on the formation of chiral nematic properties of sustainable CNCs has significant importance.

Concentrated dicarboxylic acid (DCA) hydrolysis using oxalic acid and maleic acid (MA) are promising for sustainable production of CNCs with surface carboxylation and negative charge (Chen et al., 2016; Jia et al., 2017; Wang, Chen, Zhu, & Yang, 2017). Unlike water soluble mineral acids such as sulfuric, phosphoric, and hydrochloric acids, these DCAs have low solubility that facilitates recovery (Bian et al., 2019; Cai et al., 2020). DCAs are also less corrosive than strong mineral acids, which can decrease capital and operating costs. MA is a U.S. Food and Drug Administration (FDA) approved indirect food additive (21CFR175-177) with minimal environmental impact. However, DCA-produced CNCs (DC-CNCs) are not commercially available. Limited studies have been conducted on the utility and properties of DC-CNCs (Bian et al., 2018; Chen et al., 2016). The objective of this study was to evaluate the chiral nematic property of DC-CNCs produced from cotton linter, an unusable material for textile, using concentrated DCA hydrolysis (Bian, Chen, Dai, & Zhu, 2017; Chen et al., 2016), namely MA and succinic acid (ScA). These two acids were chosen for their low solubility at atmospheric condition, which can facilitate acid recovery through crystallization (Bian et al., 2019; Cai et al., 2020). Cotton linter was used as raw material without any pretreatment due to its high cellulose content. To enhance CNC carboxylation and therefore surface charge, catalyst and dicarboxylic anhydride were used in hydrolysis reactions. The resultant CNCs were used to produce films through casting for evaluating the resultant CNC chiral nematic structure.

2. Materials and methods

2.1. Materials

Cotton linter, 10−30 μm in diameter with varied lengths from 50−1000 μm, was obtained from a commercial source. Maleic acid, maleic anhydride, succinic acid, succinic anhydride, acetic acid, and *p*-toluenesulfonic acid (*p*-TsOH) all analytical grade were purchased from Sinopharm chemical reagent Co. Ltd (Shanghai, China). Deionized (DI) water was used throughout the experiment.

2.2. Preparation of carboxylated cellulose nanocrystals

DC-CNC production followed the experimental schematic flow diagram shown in Fig. 1. In this process, 3 g cotton linter in oven dry (OD) weight were mixed with 20 g maleic acid or succinic acid, 10 g maleic anhydride or succinic anhydride, with or without *p*-TsOH (1 g), and 20 mL acetic acid as solvent (Table S1). The mixture was placed in a 250-mL three-necked flask and heated in an oil bath at 100 ℃. After stirring for 2 h, the reaction was terminated by adding 20 mL water into the flask and stirring for several minutes. The resultant mixture was then centrifuged at 10,000 rpm for 10 min. The supernatant (diluted hydrolysate) was filtrated then crystallized for later reuse. The solids were added with water for washing and centrifuged at 10,000 rpm for 10 min. This washing-centrifuging process was repeated until the supernatant was turbid. The turbid supernatant was collected and dialyzed using DI water until the pH of the dialysis water no longer changed. The DC-CNCs were finally obtained. To facilitate discussion, the DC-CNC samples were labelled as *p*-M-CNCs and M-CNCs to represent using maleic acid and maleic anhydride as reactants with and without *p*-TsOH, respectively, and *p*-Sc-CNCs and Sc-CNCs to represent using succinic acid and succinic anhydride as reactants with and without *p*-TsOH, respectively.

2.3. CNC film casting

10 mL of 11.0 wt % DC-CNC suspension was sonicated for approximately 5 min by an ultrasonic processor (model KQ5200DE, Ultrasonic Equipment Co., Ltd., Shanghai, China) with a power input of 300 W and then immediately poured into a 50-mm-diameter polystyrene Petri dish. The suspension was left undisturbed, and water was allowed to evaporate under ambient. After drying, the films were peeled off from the Petri dish for characterization.

2.4. Recovery of dicarboxylic acid

By adding water to terminate hydrolysis and washing the residue solids, the anhydrate in the hydrolysate (liquid fraction) is converted into its corresponding acid and is recovered in the acid form to result in a low pH of approximately 1.5. The hydrolysate that contains dicarboxylic acid and solvent acetic acid is separated from the solid fraction that included the cellulosic solid residue and CNCs by filtration after centrifugation as discussed in Section 2.2. The collected diluted hydrolysates were successively passed through a fine filter (pore size 0.1–1 μm, 30 × 500 mm, Chengyinuo Instrument Co., Ltd, Guangzhou,

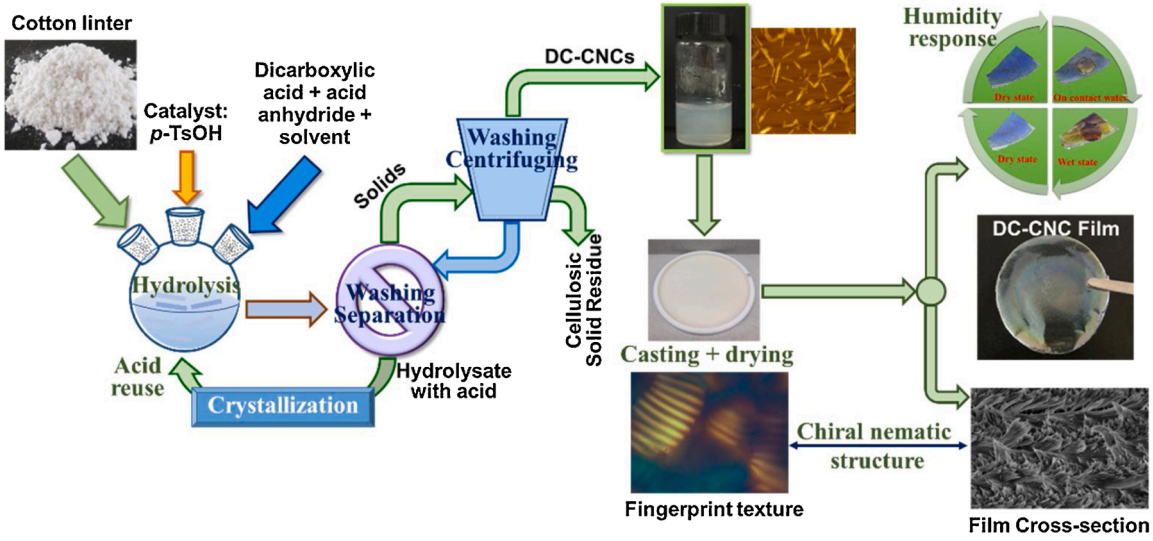

Fig. 1. Experimental schematic flow diagram showing DC-CNC and DC-CNC film production and DC-CNC film characterization.

China) and an activated carbon column to remove fine solids. After passing through the column, each hydrolysate along with the corresponding first washing filtrate was evaporated in a rotary evaporator under vacuum (−0.1 MPa) at 90 °C. A certain amount of dissolved sugars in the hydrolysate was dehydrated into furan (Cai et al., 2020), while most acetic acid and washing water were distillated. Recovery of acetic acid and furan were not carried out this study. After cooling to 4 °C, crystallization was observed. Crystals were separated in the form of wet solids from the bulk liquid. Therefore, certain amounts of acetic acid and soluble sugars will be remained in the wet solids depending upon the amount of liquids retained in the wet solids. The wet solids was then vacuum-dried at 70 °C for 24 h. Before crystallization, an aliquot of hydrolysate was collected to determine the amount of acid (M_1) by high performance liquid chromatography (HPLC) (Supplementary Information). After crystallization, the residual liquid that contains primary acetic acid and water was drained out immediately and the amount of the crystallized acid (M_2) was measured gravimetrically. The theoretical acid recovery rate (R_1) and actual recovery rate (R_2) of the dicarboxylic acids were calculated by the following equations:

$$R_1(\%) = M_1/M \times 100\% \quad (1)$$

$$R_2(\%) = M_2/M \times 100\% \quad (2)$$

Where M_1 is the mass of the dicarboxylic acid determined by HPLC, M_2 is the mass of the dicarboxylic acid that crystallized, and M is the total mass of dicarboxylic acid and acid anhydrate (converted to acid base) applied at the beginning of experiment.

The recovered dicarboxylic acid was reused for hydrolyzing fresh cotton linter to produce DC-CNCs. The required amounts of fresh anhydride and acetic acid were added. The dicarboxylic acid was recovered again and reused for a third time to evaluate its catalytic efficacy for cellulose hydrolysis.

2.5. Characterization

Images of the DC-CNC samples were acquired using an atomic force microscope (AFM) (5500, Agilent Technologies, Folsom, California, USA) in tapping mode under ambient condition. Samples were diluted to solids concentration of 0.01–0.05 wt %, deposited on a clean mica substrate, and then air-dried overnight at room temperature. Scanning electron microscopy (SEM) images of the cross-sectional morphologies of the DC-CNC films (fractured in liquid nitrogen) were also obtained (Verios G4 UC, FEI Company, Hillsboro, Oregon, USA) using an accelerating voltage of 3 kV on samples sputter-coated with gold. Polarized optical microscopy (POM) graphs of the DC-CNC suspension and films were also taken (ZYP-1000E POM, Zhongnuo, China) using crossed polarizers. The pictures and color changes of DC-CNC films were captured by a digital camera.

The crystallinities of cotton linter and DC-CNC samples were evaluated by x-ray diffraction (XRD) (Min Flex 600, Rigaku, Tokyo, Japan) with Cu K_α radiation (λ =0.154 nm). Scans were performed from 5 to 60° with a rate of 10°/min. The crystallinity index (CrI) of a cellulose sample was calculated according to the Segal method (Segal, Creely, Martin, & Conrad, 1959) with baseline subtraction:

$$CrI(\%) = \frac{I_{002} - I_{am}}{I_{002}} \times 100\% \quad (3)$$

where I_{002} corresponds to the maximum diffraction intensity of the 002 lattice and I_{am} corresponds to the intensity at $2\theta = 18°$.

Fourier transform infrared (FT-IR) spectra of cotton linter and DC-CNCs were obtained using a Nicolet AVATAR 360 FT-IR spectrophotometer (ThermoFisher Scientific, Waltham, Massachusetts, USA) equipped with a universal attenuated total reflection (ATR) probe.

The surface compositions of the esterified cellulosic materials were evaluated by x-ray photoelectron spectra (XPS ESCALAB 250, ThermoFisher Scientific). In these measurements, the C-C/ C-H component of the C1s peak was adjusted to 284.6 eV.

Thermal gravimetric analyses (TGA) of the cotton linter and the DC-CNC samples were performed using a simultaneous thermal analysis (STA) TGA system (449 F5 NETZSCH Group, Selb, Germany). The temperature range was from ambient to 450 °C with a heating rate of 10 °C/ min under nitrogen. Approximately 5 mg of dried sample were used for each test.

Carboxyl group contents of DC-CNC samples were measured by conductometric titration (da Silva Perez, Montanari, & Vignon, 2003). Approximately 0.1 g DC-CNC samples were dispersed into 100 mL of 1 mL HCl solution. After stirring for 30 min, the suspension was titrated by adding 0.2 mL of a NaOH solution dropwise in 30-second intervals using a conductance meter (916 Ti-Touch, Metrohm AG, Herisau, Switzerland). The carboxyl group content of the samples was given by the following equation:

$$m_{[COOH]} = \frac{V \times C_{NaOH}}{m_{DC-CNCs}} \quad (4)$$

where V is the volume of NaOH consumed (mL), C_{NaOH} =1 mol/L, and $m_{DC\text{-}CNCs}$ is the dry weight of the DC-CNC sample (g).

The ζ potentials of the DC-CNC samples were measured on a Zeta potential analyzer (NanoBrook Omni, Brookhaven Instruments Corporation, Holtsville, New York, USA) at a concentration of 0.05 wt % in PALS mode. DI water was used as dispersant. The ζ potential was calculated using the Smoluchowski equation (Tockary et al., 2013).

3. Results and discussions

3.1. Characteristics of the DC-CNCs

Simultaneous hydrolysis and esterification of cellulose took place during DC-CNC production. The anhydride and the catalyst both enhanced CNC surface esterification, as revealed previously (Wang et al., 2017). The *p*-TsOH used in this study acted not only as a catalyst for esterification but also the source of hydronium ions that promoted the hydrolysis of cotton linter. The morphologies of DC-CNC samples prepared by the two dicarboxylic acids with or without *p*-TsOH were observed by AFM (Fig. 2A–D). The four DC-CNC samples were not significantly different with dimensions mostly from 50 to 700 nm in length but varied in heights (diameters) based on AFM topographic measurements (Fig. 2E and F) with mean values of 70–110 nm (Table 1). The AFM topography measured CNC heights clearly indicate that most CNCs are crystal aggregates that can be seen from the AFM images especially the two CNC samples without *p*-TsOH (Fig. 2A and B). It is well known that the average diameters of sulfuric acid CNCs are approximately 10 nm with a range from 3 to 50 nm (Wang et al., 2012) and length from 10 to 400 nm (Chen et al., 2015), and are therefore crystal aggregates. The weak acidities of the DCAs certainly resulted in CNCs with greater aggregation and diameters and lengths than sulfuric acid CNCs. It appears that the CNC height distributions (comparing Fig. 2E with F) and the mean heights of M-CNCs and Sc-CNCs are not significantly different (Table 1). However, the low acidity of ScA (pKa1 = 4.2, compared with MA pKa1 = 1.9) resulted in a lower CNC yield of 11 % than MA of 22 %, and lower CNC carboxyl groups content of 0.53 mmol/g than 0.64 mmol/g from MA (Table 1).

By examining Fig. 2E and F and comparing Fig. 2A with C and Fig. 2B with D, it can be concluded that the application of *p*-TsOH promoted the hydrolysis of the cotton linter and the separation of crystals with more uniform CNC dimensions. Furthermore, *p*-TsOH is more effective with MA than with ScA in enhancing hydrolysis as can be seen from the mean height of *p*-M-CNCs of 72 nm compared with *p*-Sc-CNCs of 92 nm and the shift of the height distribution peak from approximately 65 nm for *p*-M-CNCs (Fig. 2E) to 80 nm for *p*-Sc-CNCs (Fig. 2F). *p*-TsOH also significantly increased CNC carboxylation and yield for both MA and ScA

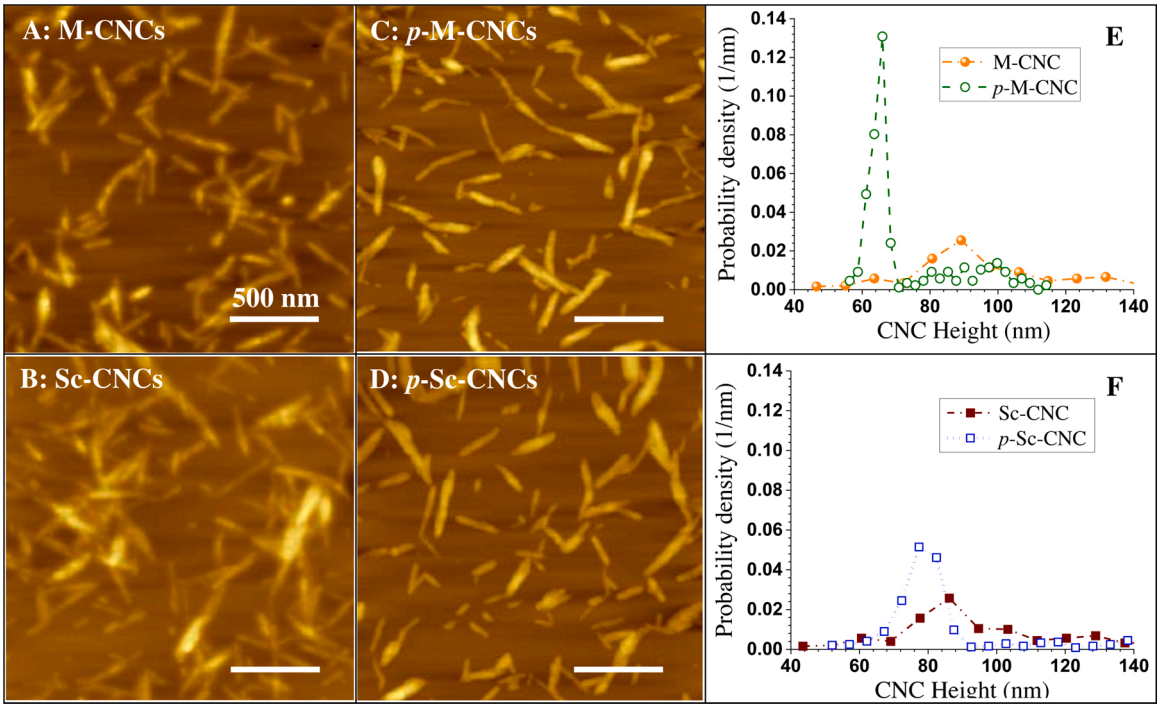

Fig. 2. AFM images (A-D) and AFM topography measured height distributions (E and F) of the DC-CNCs produced from cotton linter using maleic and succinic acid with or without *p*-TsOH. All scale bars =500 nm.

Table 1
Morphological, physical, and chemical properties, along with critical concentrations for the formation of liquid crystal phase (CC1) and fingerprint texture (CC2) of DC-CNCs.

Samples	Cotton linter	M-CNCs	*p*-M-CNCs	Sc-CNCs	*p*-Sc-CNCs
Yield (%)	–	22	28	11	17
Mean height (nm)	–	110	72	107	92
Aspect ratio		5 – 50	10 – 90	6 – 64	5 – 55
Carboxyl groups (mmol/g)	–	0.64	0.89	0.53	0.75
ζ potential (mV)	–	−38 ± 3	−53 ± 2	−32 ± 2	−51 ± 4
CrI (%)	74.5 ± 5.2	79.6 ± 2.3	76.8 ± 2.6	77.7 ± 4.3	75.5 ± 3.7
CC1(%)		4.8	4.2	5.1	4.6
CC2(%)		–	9.0	–	11.0

(Table 1). The low CNC yields for all four runs can be attributed to the weak acidity of the two DCAs than sulfuric acid, in agreement with previous studies using bleached wood fibers (Chen et al., 2016; Wang et al., 2017). However, the overall yield of cellulose solid is high of over 90 %, or degradation of cellulose to sugar was minimal. The cellulose solid residue can be easily fibrillated into cellulose nanofibrils, another high value cellulose nanomaterials as demonstrated previously (Chen et al., 2016; Wang et al., 2017). This is very different from most sulfuric acid hydrolysis studies that resulted a CNC yield of 50 % with remaining cellulose degraded into monomeric sugars that is low value and difficult to recover. DC-CNC yield can be improved by increasing reaction temperature to 120 °C and premilling the cotton linter as demonstred previously (Chen et al., 2016; Jia et al., 2017). The four DC-CNC suspensions in neutral water all had negative zeta potentials (Table 1) due to the presence of the negatively charged carboxyl groups on their surface, which ensures their dispersion to result in stable aqueous suspensions.

The four DC-CNC samples all showed typical XRD patterns of cellulose I (Fig. 3A), with the main diffraction peaks at 2θ = 14.8°, 16.2°, and 22.7°, assigned to the ($1\bar{0}1$), (101), and (002) planes, respectively. Compared with that of cotton linter, all the DC-CNC samples had a slightly higher *CrI* (Table 1) due to hydrolysis of disordered cellulose. The two DC-CNC samples from MA hydrolysis, M-CNCs and *p*-M-CNCs, have higher *CrI* than their corresponding DC-CNC samples from ScA hydrolysis, Sc-CNCs and *p*-Sc-CNCs. This is due to the stronger acidity of MA than ScA that resulted in improved hydrolysis of disordered cellulose. Application of catalyst *p*-TsOH, however slightly reduced *CrI*.

Thermal stabilities of the DC-CNC samples were also evaluated as shown in Fig. 3B. Table S2 gives values for T_{onset} (defined as dW/dT = −1 (Chen et al., 2016)), T_{max} (maximal weight loss temperature), and T_{95} (defined as 5 % weight loss). Acid hydrolysis decreased thermal stability as can be clearly seen by comparing the data for the CNC samples with the data of cotton linter, this is especially true for the two CNC samples from ScA hydrolysis. The lower thermal stability of DC-CNCs compared with that of the unprocessed cotton linter can be attributed to the carboxyl groups, which decompose at lower temperatures than do hydroxyl groups (Ji et al., 2019). It can also be attributed to the substantially greater surface area of CNCs and decreased cellulose degree of polymerization (Vanderfleet et al., 2019) than the cotton linter. The decrease in thermal stability of the two M-CNC samples by MA hydrolysis was minimal compared with that of cotton linter. These two DC-CNC samples, M-CNCs and *p*-M-CNCs, had much greater thermal stability than the two Sc-CNC samples from ScA hydrolysis, Sc-CNCs and *p*-Sc-CNCs. This can be attributed to the higher crystallinities of the MA hydrolysis DC-CNCs than ScA hydrolysis DC-CNCs (Table 1) (Chen et al., 2016). It appears that catalyst *p*-TsOH had negligible effect on resultant CNC thermal stability.

The presence of carboxyl groups on DC-CNCs was also confirmed by Fourier transform infrared (FTIR) spectroscopy. Compared with the cotton linter, the FTIR spectra of DC-CNC samples had a new peak at 1728 cm^{-1} (Fig. 3C) that is attributed to the carbonyl groups (C═O) or carboxyl groups, qualitatively verified by titration measurements (Table 1).

XPS was used to determine the nature of superficial atoms. Both the

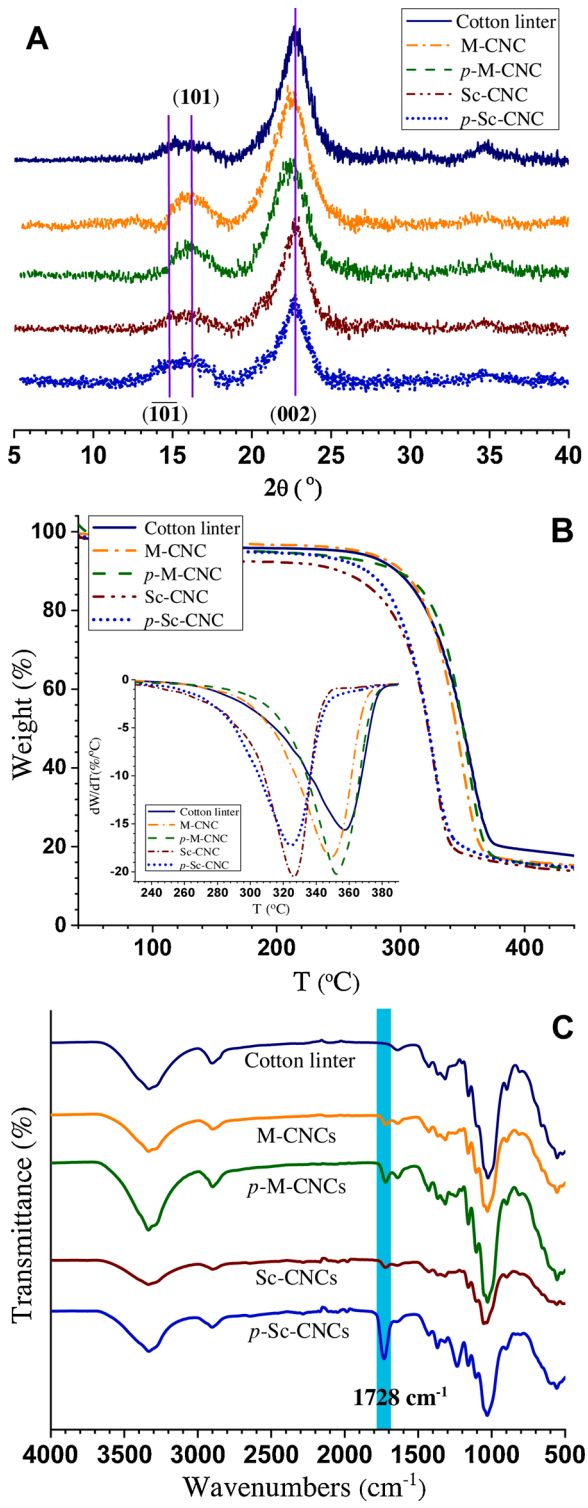

Fig. 3. Comparisons of DC-CNC samples with unprocessed cotton linter through x-ray diffraction (A), thermal gravimetric (B), and FTIR (C) analyses.

cotton linter and DC-CNCs displayed two principal peaks at approximately 533 eV and 285 eV in XPS spectra (Fig. 4A), corresponding to oxygen and carbon, respectively. However, the deconvolution of the C1s high-resolution signal highlighted the differences between the cotton linter and DC-CNC samples (Fig. 4B–D). The C1s peak of all the samples were fitted with four components according to the peak assignment by (Dorris & Gray, 1978). The peak at 284.6 eV is assigned to C—C and C—H bonds (C1), the peaks around 286.3 eV and 288.0 eV were often assigned to C—OH and O—C—O/C═O (C2 and C3), respectively. And the DC-CNC samples exhibited a fourth peak at approximately 289.0 eV from C═O groups (C4), further confirming the presence of carboxyl group on the DC-CNC surface.

3.2. Chiral nematic properties of DC-CNCs

It is well known that, above critical concentrations, suspensions of CNCs produced from concentrated sulfuric acid hydrolysis exhibit liquid crystal properties (Revol et al., 1992). The generated crystalline phase was normally cholesteric liquid crystal, also called the chiral nematic phase. Here, we found that DC-CNC suspensions also form a chiral nematic phase. However, different behavior was expected due to the differences in CNC morphology (Elazzouzi-Hafraoui et al., 2009) and surface charge groups, i.e., longer CNC length with larger diameters and carboxy groups in DC-CNCs instead of shorter length with thiner diameters and sulfate half-ester groups, compared with sulfuric-acid-produced CNCs.

Birefringence, the most important optical property caused by the loss of physical isotropy when CNCs self-organize in a suspension, was first used to assess whether the liquid crystal phase was formed. DC-CNC suspensions of varied concentrations were prepared for each DC-CNC sample and then observed by POM. Fig. 5A showed the POM images of M-CNC suspension at concentrations of 3.2 wt %, 4.8 wt %, and 9.0 wt % under different rotation angles (0° and 45°) of the objective stage. No changes in color were observed at two rotation angles (0° and 45°) for the suspension at 3.2 wt %, implying optical isotropy. However, when the concentration was increased to 4.8 wt %, birefringence was apparent. As the concentration further increased to 9.0 wt %, the birefringence became more intense. Similar birefringence behavior was also observed for the other three DC-CNC samples as shown in Fig. 5C–D. Using the same method, the critical concentrations (*CC1*) for *p*-M-CNCs, Sc-CNCs, and *p*-Sc-CNCs were obtained, i.e., 4.2 wt %, 5.1 wt %, and 4.6 wt %, respectively. The results were summarized in Table 1, and the values were consistent with the those of CNCs prepared using sulfuric acid hydrolysis (Revol et al., 1992). *p*-M-CNCs with the highest aspect ratio and carboxyl content has the lowest critical concentrations among the four DC-CNC samples. It has been reported that both the aspect ratio and the surface charges have an impact on the critical concentration for the formation of the liquid crystal phase (Beck-Candanedo, Roman, & Gray, 2005; Dong, Kimura, Revol, & Gray, 1996; Stroobants, Lekkerkerker, & Odijk, 1986). Increasing aspect ratio decreases the critical concentration (Elazzouzi-Hafraoui et al., 2009; Onsager, 1949), whereas increasing carboxyl group content, i.e., surface charge, increases electrostatic repulsion, which facilitates the parallel alignment of CNCs to form the liquid crystal phase at low concentrations (Hanaor et al., 2011; Liu et al., 2016).

3.3. Fingerprint pattern characteristic

With increasing concentration, the particles of ordered phase (sometimes called tactoids) could gradually emerge to form a fingerprint texture, which is a characteristic of chiral nematic liquid crystals. The POM images between crossed polarizations of DC-CNC suspensions above the critical concentrations are presented in Fig. 6. A well-oriented liquid crystalline phase with clear tactoids was first observed at concentrations 9.0 wt % and 11.0 wt % for *p*-M-CNC and *p*-Sc-CNC suspensions, respectively, indicating the formation of the CNC chiral nematic liquid phase. However, no clear evidence of the ordered phase was observed in the suspensions of M-CNCs and Sc-CNCs produced without catalyst *p*-TsOH even above concentration 17 wt % after evaporation for a couple of hours. Perhaps, this is due to the lower carboxyl group content or surface charge and greater polydispersity in physical dimensions of these two DC-CNC samples compared with their corresponding samples produced with catalyst *p*-TsOH (Fig. 2 and Table 1). The critical CNC suspension concentrations for the formation of

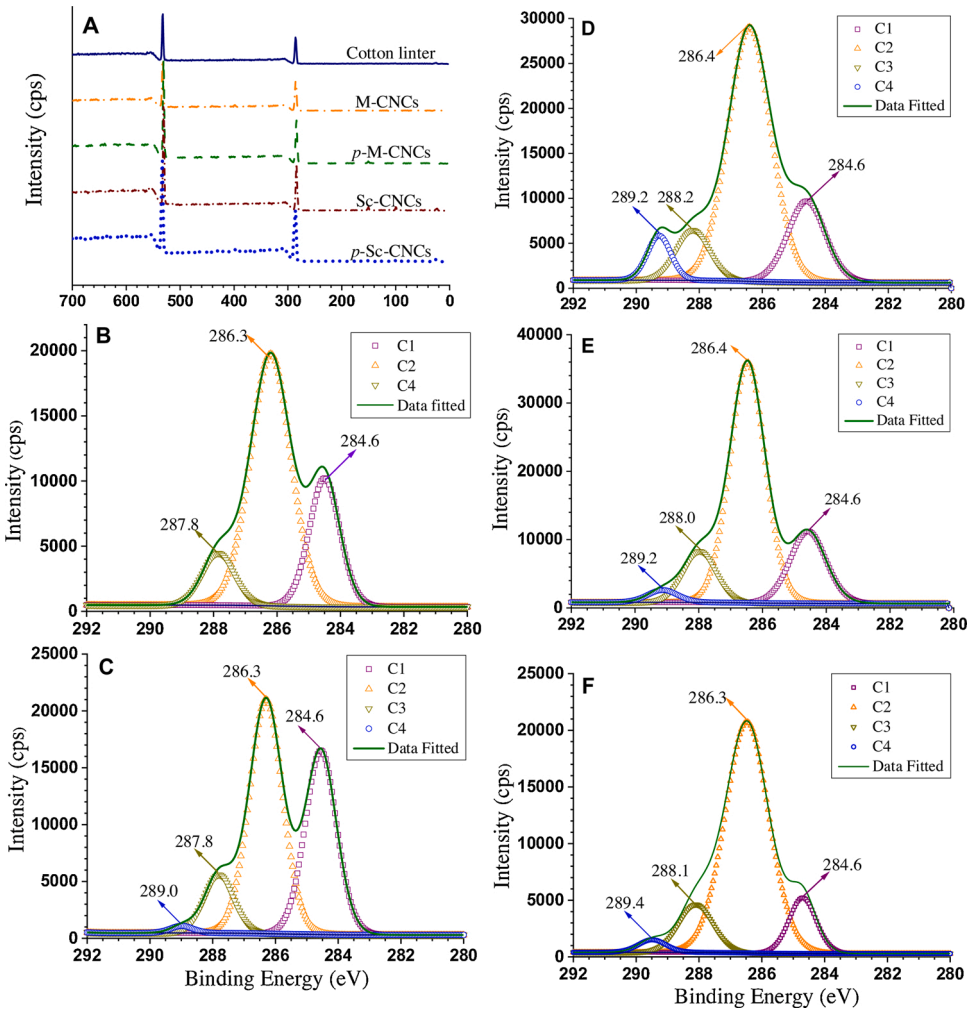

Fig. 4. A: XPS spectra of all DC-CNC samples and the unprocessed cotton linter. B-F: Deconvolution of the C1 peaks of the C-CNC samples and the cotton linter: cotton linter (B); M-CNCs (C); *p*-M-CNCs (D); Sc-CNCs (E); and *p*-Sc-CNCs (F).

fingerprint texture (*CC2*) are listed in Table 1. In general, DC-CNCs tend to aggregate and form a gel rather than an ordered phase (Jia & Liu, 2019).

The chiral nematic pitch *P*, more commonly used in its reciprocal value 1/*P*, defined as the distance between CNC rods with the same orientation after a complete 360° rotation, was used to evaluate the chiral interaction between crystals (Dong & Gray, 1997). *P* is commonly determined by measuring the distance between three successive dark (or light) bands of the fingerprint texture in a POM image (Castro-Guerrero & Gray, 2014; Elazzouzi-Hafraoui et al., 2009). *P* was 40.0 μm and 33.2 μm at the beginning of the appearance of tactoids (top row in Fig. 6B and D) for *p*-M-CNC and *p*-Sc-CNC suspensions, respectively, and then decreased quickly to 7.0 μm and 6.0 μm in approximately 10 min (bottom row of Fig. 6B and D), respectively. The reduction in P with time can be attributed to spontaneous relaxation of the chiral nematic phase (Khadem, Bagnani, Mezzenga, & Rey, 2020). The terminal (equilibrium) *P* values were smaller than those reported in the literature for CNCs produced using sulfuric acid hydrolysis of 30−60 μm (Dong et al., 1996; Revol et al., 1992). The helical pitch of the chiral nematic crystal liquid was influenced by various factors, such as surface charges, CNC concentration, nanocrystal size, etc. In addition, increasing CNC concentration, such as through evaporation of water in suspension, decreases pitch (Castro-Guerrero & Gray, 2014). Sonication can release some of the ions trapped in the bound-water layer on the surface of CNC particles, leading to an increase in *P* due to the increase in electrostatic repulsion between CNC particles as supported by the increase in suspension conductivity (Fig. S1).

3.4. DC-CNC films

The appearance of DC-CNC films prepared by evaporation-induced self-assembly under natural light are shown in Fig. 7A. Both M-CNC (12 μm thickness) and Sc-CNC (21 μm thickness) films were somewhat transparent and not very iridescent, whereas *p*-M-CNC (9 μm thickness) and *p*-Sc-CNC (54 μm thickness) films displayed iridescent color. The planar texture was observed by POM in *p*-M-CNC and *p*-Sc-CNC films (Fig. 7B), indicating the preservation of organized helical structure in solid films. The *P* were measured as 1.0–3.0 μm and 2.0–6.0 μm for *p*-M-CNC and *p*-Sc-CNC films, respectively, much less than that of the corresponding suspensions due to water evaporation. SEM images of the cross section of *p*-M-CNC and *p*-Sc-CNC films clearly show more uniform and better ordered multilayered structure compared with M-CNC and Sc-CNC films (Fig. 7C). Magnifying the SEM images can better reveal the layered structure and orientation of CNCs (Fig. 7D). The calculated helical pitch of the *p*-M-CNC film was approximately 2 μm, which is consistent with those measured by POM. It should be noted that the thickness of the film only affects the light reflectivity and spectral bandwidth, but does not affect the pitch values (Liu et al., 2014).

It is widely known that the chiral nematic property of CNC films is sensitive to humidity (Parker et al., 2018). The *p*-M-CNC film in a dry state showed strong blue reflection under natural light (Fig. 8A). After wetting the film with a water drop on the surface, the color of the film

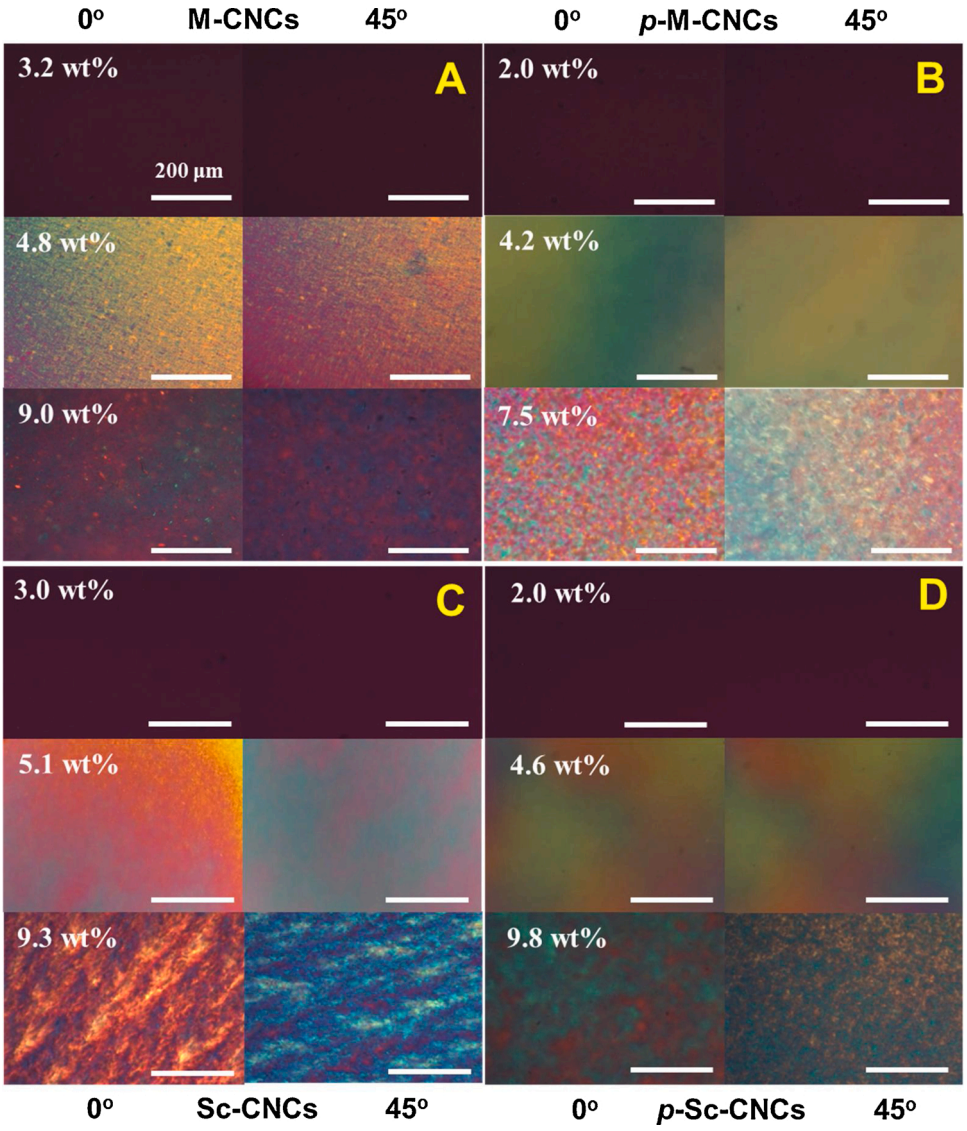

Fig. 5. POM micrographs of DC-CNC suspensions at different concentrations under 0° and 45° rotation angles of the objective stage. All scale bars =200 μm. A: M-CNCs; B: *p*-M-CNCs; C: Sc-CNCs; D: *p*-Sc-CNCs.

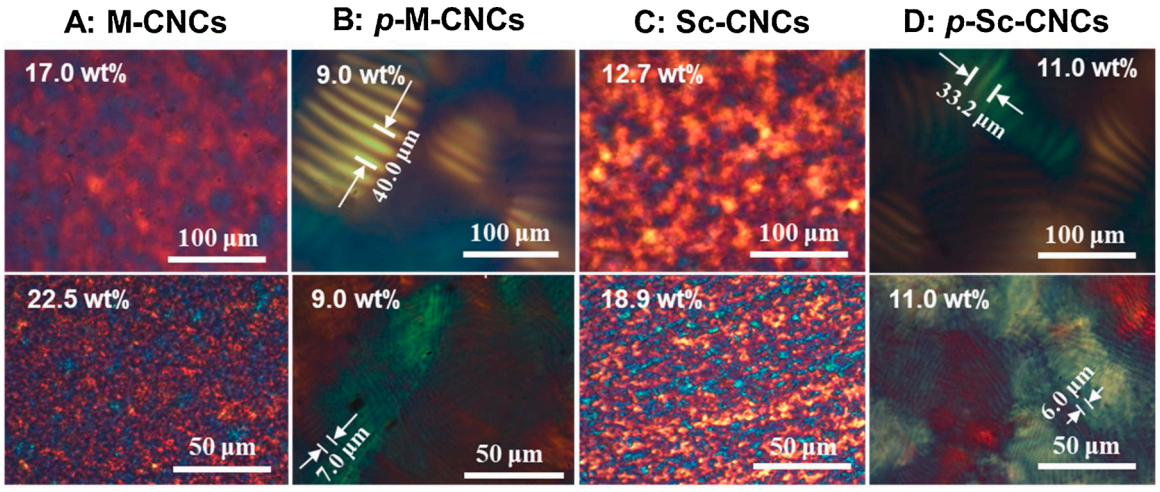

Fig. 6. POM micrographs of DC-CNC suspensions above the critical concentration to form fingerprint texture (C2). A: M-CNCs; B: *p*-M-CNCs; C: Sc-CNCs; D: *p*-Sc-CNCs. B and D: the images in the bottom rows were taken 10 min after taking the images in the top row.

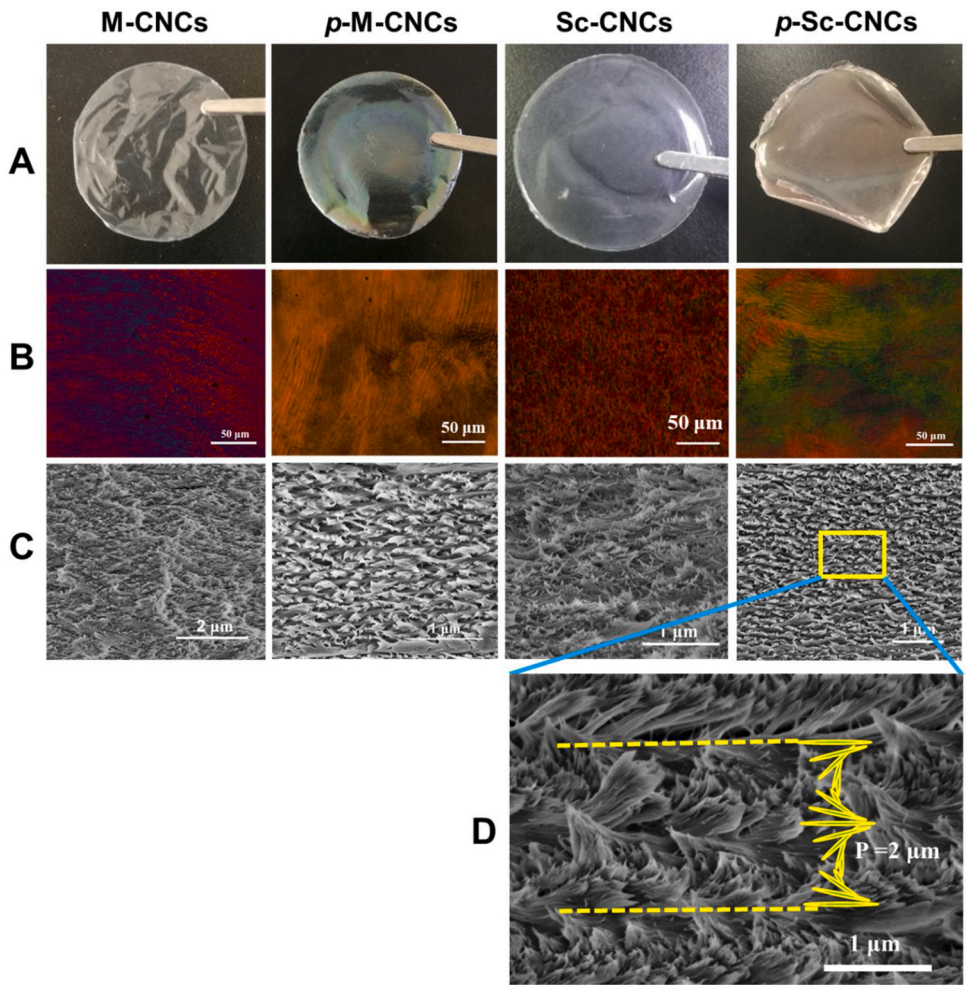

Fig. 7. A: Photographs of DC-CNC films; B: POM images of DC-CNC films taken with crossed polarizers; C: SEM images of the cross sections of DC-CNC films; D: Magnified view of the layered structure within the cross section of the *p*-Sc-CNC film shown in C.

gradually changed from blue to yellow and then to red (highest humidity within the water drop region, insets in Fig. 8B and C). However, the blue color was recovered (inset of Fig. 8D) after the removal of water and drying. This process was carried out repeatedly and the spectral response was recorded (Fig. S2). The fingerprint structure of the films before and after water absorption were illustrated by POM. The images shown in Fig. 8 reveal the changes in the pitch of the film throughout the wetting and redrying process. The pitch was approximately 1.0–4.0 μm in its initial dry state (Fig. 8A) and was increased to approximately 20.0–40.0 μm in the wet state (Fig. 8C). The pitch was recovered to 1.0–4.0 μm again after water removal and redrying (Fig. 8D). According to the Bragg's reflection equation of crystal diffraction (Eq. 5) (Vries, 1951), there was a linear relationship between the maximum reaction wavelength and cholesteric pitch:

$$\lambda_{max} = n_{av} \times P \times \sin\theta \quad (5)$$

where λ_{max} and n_{av} are reflectance peak and average refractive index of the film, respectively, P is the pitch of the helical structure, and θ is the angle of light incident on the film surface. Therefore, the increase in P leads to a red shift in the reflectance peak of the film (increase in λ_{max}). In other words, the color of the film changes as wetting and water evaporation with time, showing great potential application in such areas of anti-counterfeiting and humidity sensing.

3.5. Effect of DCA recycling on the properties of DC-CNCs

Compared with the other methods that are used to prepare carboxylated CNCs (Leung et al., 2011; Zhou et al., 2018), the reaction time of the DCA hydrolysis method is the shortest (approximately 1–2 h). The main advantage lies in the recyclability of the dicarboxylic acids due to their low solubility. Evaluation of acid recovery can be found in the Support Information (Figs. S3-S4). The results confirmed the high recovery rate and structural stability of the dicarboxylic acids through being recycled multiple times. However, the DC-CNCs, *p*-M-CNCs, and *p*-Sc-CNCs produced using recycled acids with catalyst *p*-TsOH had a lower surface charge and a lower carboxyl group content than the corresponding values of the samples produced using fresh acids (Table S3). The decreases were not apparent for the DC-CNCs without catalyst *p*-TsOH, suggesting the decreases were perhaps caused by the loss of *p*-TsOH, which was removed with the removal of water and solvent acetic acid because *p*-TsOH is more soluble than the two dicarboxylic acids studied here. Morphological variations among DC-CNCs from using acid recycled multiple times and from the sample using fresh acid were observed. The observed variations by AFM (Fig. S5) can be due to variations in sampling as well as due to variations in the chemical composition of the recycled chemicals. Further study is in progress to achieve true sustainable production of DC-CNCs with the use of these dicarboxylic acids with low environmental impact.

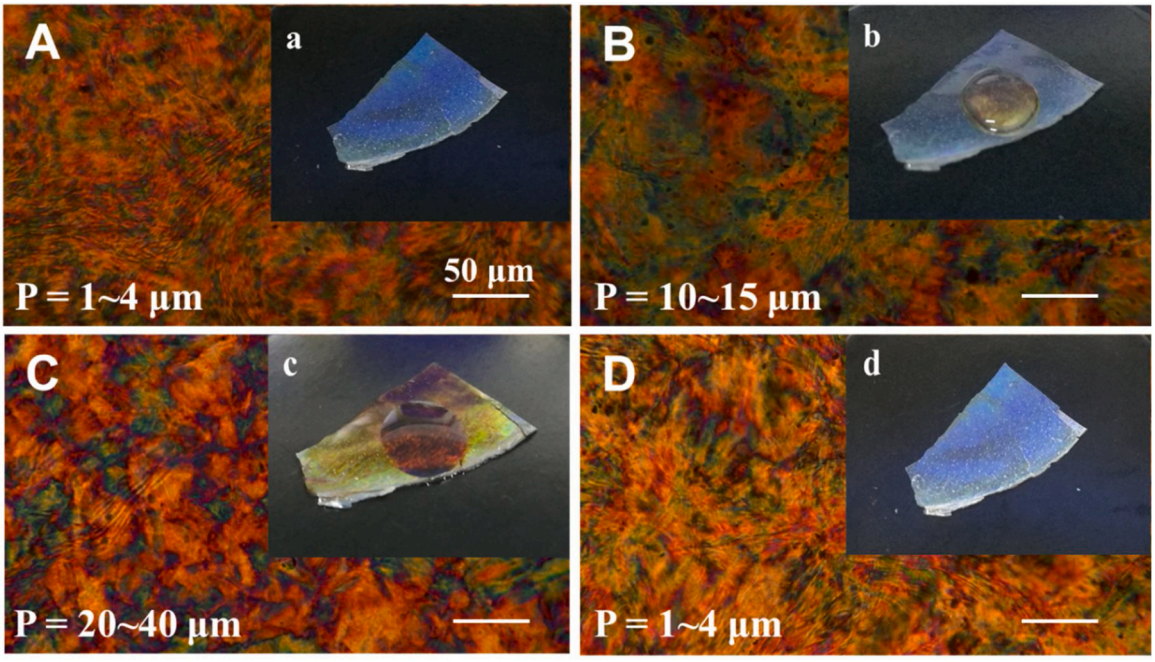

Fig. 8. POM images of a *p*-M-CNC film in dry and wet states. All scale bars =50 μm. A: dry state; B: at the beginning of contacting a water drop (t = 0); C: after moisture absorption (t =5 min); D: after water removal and redrying (t =30 min). All insets are photographs of the CNC films under natural light in dry and during wet states.

4. Conclusions

DC-CNCs from cotton linter with chiral nematic properties can be prepared through hydrolysis and esterification in one pot using maleic or succinic acid mixed with their respective dicarboxylic acid anhydrates to enhance esterification with or without a catalyst of *p*-TsOH. Detailed morphological and chemical structural analyses of the as-prepared DC-CNC samples showed the rod-like shape of DC-CNC samples with surface charges from cellulose surface esterification. The liquid crystal phase was formed in the suspensions of DC-CNCs above critical concentrations. The fingerprint texture was also clearly observed from the suspensions of two DC-CNC samples, *p*-M-CNCs and *p*-Sc-CNCs, produced with catalyst *p*-TsOH at concentrations of 9.0 % and 11.0 %, respectively. SEM images of the cross section of DC-CNC films displayed a clear chiral nematic characteristic. Reversible color change of the DC-CNC films due to moisture change was also observed. The recyclability of the two dicarboxylic acids was also demonstrated to achieve process sustainability compared with the conventional concentrated sulfuric acid hydrolysis process.

CRediT authorship contribution statement

J.Y. Zhu: developed the concept of the study and contributed the major revisions of the manuscript. **Chunxiang Lin:** conducted major parts of the study and drafted the manuscript. **Beiqiu Chen** and **Yushi Liu:** contributed to sample characterizations using FE-SEM, XRD, XPS, AFM, and POM. **Yiting Chen:** did the thermal stability tests. **Minghua Liu:** contributed to the interpretation and data analyses.

Declaration of Competing Interest

Zhu is the co-inventor of the dicarboxylic acid hydrolysis process for producing DC-CNCs.

Acknowledgements

This work was sponsored by the Natural Science Foundation of Fujian Province, China, (grant no. 2020J01506) and the Open Project Program of Fujian Provincial University Engineering Research Center of Green Materials and Chemical Engineering, Minjiang University, China (grant no. MJXY-KF-CH1905).

Appendix A. Supplementary data

Supplementary material related to this article can be found, in the online version, at doi:https://doi.org/10.1016/j.carbpol.2021.118039.

References

Azzam, F., Heux, L., & Jean, B. (2016). Adjustment of the chiral nematic phase properties of cellulose nanocrystals by polymer grafting. *Langmuir, 32*(17), 4305–4312.

Beck-Candanedo, S., Roman, M., & Gray, D. G. (2005). Effect of reaction conditions on the properties and behavior of wood cellulose nanocrystal suspensions. *Biomacromolecules, 6*, 1048–1054.

Bian, H., Chen, L., Dai, H., & Zhu, J. Y. (2017). Integrated production of lignin containing cellulose nanocrystals (LCNC) and nanofibrils (LCNF) using an easily recyclable dicarboxylic acid. *Carbohydrate Polymers, 167*, 167–176. https://doi.org/10.1016/j.carbpol.2017.03.050

Bian, H., Luo, J., Wang, R., Zhou, X., Ni, S., Shi, R., et al. (2019). Recyclable and reusable maleic acid for efficient production of cellulose nanofibrils with stable performance. *ACS Sustainable Chemistry & Engineering 7*, 20022–20031. https://doi.org/10.1021/acssuschemeng.9b05766

Bian, H., Wei, L., Lin, C., Ma, Q., Dai, H., & Zhu, J. Y. (2018). Lignin-containing cellulose nanofibril-reinforced polyvinyl alcohol hydrogels. *ACS Sustainable Chemistry & Engineering, 6*(4), 4821–4828. https://doi.org/10.1021/acssuschemeng.7b04172

Cai, C., Li, J., Hirth, K., Huber, G. W., Lou, H., & Zhu, J. Y. (2020). Comparison of two acid hydrotropes for sustainabl fractionation of birch wood. *ChemSusChem, 13*, 4649–4659. https://doi.org/10.1002/cssc.202001120

Castro-Guerrero, C. F., & Gray, D. G. (2014). Chiral nematic phase formation by aqueous suspensions of cellulose nanocrystals prepared by oxidation with ammonium persulfate. *Cellulose, 21*(4), 2567–2577.

Chen, L., Wang, Q., Hirth, K., Baez, C., Agarwal, U. P., & Zhu, J. Y. (2015). Tailoring the yield and characteristics of wood cellulose nanocrystals (CNC) using concentrated acid hydrolysis. *Cellulose, 22*, 1753–1762. https://doi.org/10.1007/s10570-015-0615-1

Chen, L., Zhu, J. Y., Baez, C., Kitin, P., & Elder, T. (2016). Highly thermal-stable and functional cellulose nanocrystals and nanofibrils produced using fully recyclable organic acids. *Green Chemistry, 18*, 3835–3843. https://doi.org/10.1039/C6GC00687F

Cheng, Z., Ye, H., Cheng, F., Li, H., Ma, Y., Zhang, Q., et al. (2019). Tuning chiral nematic pitch of bioresourced photonic films via coupling organic acid hydrolysis. *Advanced Materials Interfaces, 6*(7).

da Silva Perez, D., Montanari, S., & Vignon, M. R. (2003). TEMPO-mediated oxidation of cellulose III. *Biomacromolecules, 4*(5), 1417–1425.
Dong, X. M., & Gray, D. G. (1997). Induced circular dichroism of isotropic and magnetically-oriented chiral nematic suspensions of cellulose crystallites. *Langmuir, 13*(11), 3029–3034.
Dong, X. M., Kimura, T., Revol, J., & Gray, G. D. (1996). Effects of ionic strength on the isotropic-chiral nematic phase transition of suspensions of cellulose crystallites. *Langmuir, 12*, 2076–2082. https://doi.org/10.1021/la950133b
Dong, X. M., Revol, J. F., & Gray, D. G. (1998). Effect of microcrystallite preparation conditions on the formation of colloid crystals of cellulose. *Cellulose, 5*, 19–32.
Dorris, G. M., & Gray, D. G. (1978). The surface analysis of paper and wood fibers by ESCA., 2021ESCA. I.I. Surface composition of mechanical pulps. *Cellulose Chem. & Technol., 12*, 721–734.
Dumanli, A. G., Van Der Kooij, H. M., Kamita, G., Reisner, E., Baumberg, J. J., Steiner, U., et al. (2014). Digital color in cellulose nanocrystal films. *ACS Applied Materials & Interfaces, 6*(15), 12302–12306.
Elazzouzi-Hafraoui, S., Putaux, J. L., & Heux, L. (2009). Self-assembling and chiral nematic properties of organophilic cellulose nanocrystals. *The Journal of Physical Chemistry B, 113*(32), 11069–11075.
Giese, M., Blusch, L. K., Khan, M. K., & MacLachlan, M. J. (2015). Functional materials from cellulose-derived liquid-crystal templates. *Angewandte Chemie International Edition in English, 54*, 2888–2910.
Hanaor, D., Michelazzi, M., Veronesi, P., Leonelli, C., Romagnoli, M., & Sorrell, C. (2011). Anodic aqueous electrophoretic deposition of titanium dioxide using carboxylic acids as dispersing agents. *Journal of the European Ceramic Society, 31*(6), 1041–1047.
Hu, Z. H., Omer, A. M., Ouyang, X. K., & Yu, D. (2018). Fabrication of carboxylated cellulose nanocrystal/sodium alginate hydrogel beads for adsorption of Pb(II) from aqueous solution. *International Journal of Biological Macromolecules, 108*, 149–157.
Ji, H., Xiang, Z., Qi, H., Han, T., Pranovich, A., & Song, T. (2019). Strategy towards one-step preparation of carboxylic cellulose nanocrystals and nanofibrils with high yield, carboxylation and highly stable dispersibility using innocuous citric acid. *Green Chemistry, 21*(8), 1956–1964.
Jia, W., & Liu, Y. (2019). Two characteristic cellulose nanocrystals (CNCs) obtained from oxalic acid and sulfuric acid processing. *Cellulose, 26*(15), 8351–8365.
Jia, C., Chen, L., Shao, Z., Agarwal, U. P., Hu, L., & Zhu, J. Y. (2017). Using a fully recyclable dicarboxylic acid for producing dispersible and thermally stable cellulose nanomaterials from different cellulosic sources. *Cellulose, 24*, 2483–2498. https://doi.org/10.1007/s10570-017-1277-y
Kelly, J. A., Shukaliak, A. M., Cheung, C. C. Y., Shopsowitz, K. E., Hamad, W. Y., & MacLachlan, M. J. (2013). Responsive photonic hydrogels based on nanocrystalline cellulose. *Angew. Chem. Int. Ed., 52*(34), 8912–8916.
Khadem, S. A., Bagnani, M., Mezzenga, R., & Rey, A. D. (2020). Relaxation dynamics in bio-colloidal cholesteric liquid crystals confined to cylindrical geometry. *Nature Communications, 11*(1), 4616. https://doi.org/10.1038/s41467-020-18421-9
Kumar, A., I Matari, I. A., & Han, S. S. (2020). 3D printable carboxylated cellulose nanocrystal-reinforced hydrogel inks for tissue engineering. *Biofabrication, 12*(2).
Leung, A. C. W., Hrapovic, S., Lam, E., Liu, Y., Male, K. B., Mahmoud, K. A., et al. (2011). Characteristics and properties of carboxylated cellulose nanocrystals prepared from a novel one-step procedure. *Small, 7*(3), 302–305.
Liu, D., Wang, S., Ma, Z., Tian, D., Gu, M., & Lin, F. (2014). Structure-color mechanism of iridescent cellulose nanocrystal films. *RSC Advances, 4*(74), 39322–39331.
Liu, M., Liu, Y., Zhang, G., Peng, Z., Li, D., Ma, J., et al. (2016). Organic holographic polymer dispersed liquid crystal distributed feedback laser from different diffraction orders. *Journal of Physics D: Applied Physics, 49*(46).
Onsager, L. (1949). Statistical hydrodynamics. *Il Nuovo Cimento Series 9, 6*(2 Supplement), 279–287.
Parker, R. M., Guidetti, G., Williams, C. A., Zhao, T., Narkevicius, A., Vignolini, S., et al. (2018). The self-assembly of cellulose nanocrystals: Hierarchical design of visual appearance. *Advanced Materials, 30*(19).
Revol, J.-F., Bradford, H., Giasson, J., Marchessault, R. H., & Gray, D. G. (1992). Helicoidal self-ordering of cellulose microfibrils in aqueous suspension. *International Journal of Biological Macromolecules, 14*, 170–172.
Revol, J.-F., Godbout, L., Dong, X.-M., Gray, D. G., Chanzy, H., & Maret, G. (1994). Chiral nematic suspensions of cellulose crystallites; phase separation and magnetic field orientation. *Liquid Crystals, 16*, 127–134.
Roman, M., & Winter, W. T. (2004). Effect of sulfate groups from sulfuric acid hydrolysis on the thermal degradation behavior of bacterial cellulose. *Biomacromolecules, 5*(5), 1671–1677.
Segal, L., Creely, J. J., Martin, A. E., & Conrad, C. M. (1959). An empirical method for estimating the degree of crystallinity of native cellulose using the X-ray diffractometer. *Text. Res. J., 29*, 786–794.
Stroobants, A., Lekkerkerker, H. N. W., & Odijk, T. (1986). Effect of electrostatic interaction on the liquid crystal phase transition in solutions of rodlike polyelectrolytes. *Macromolecules, 19*(8), 2232–2238.
Tockary, T. A., Osada, K., Chen, Q., MacHitani, K., Dirisala, A., Uchida, S., et al. (2013). Tethered PEG crowdedness determining shape and blood circulation profile of polyplex micelle gene carriers. *Macromolecules, 46*(16), 6585–6592.
Vanderfleet, O. M., Reid, M. S., Bras, J., Heux, L., Godoy-Vargas, J., Panga, M. K. R., et al. (2019). Insight into thermal stability of cellulose nanocrystals from new hydrolysis methods with acid blends. *Cellulose, 26*(1), 507–528.
Vries, H. D. (1951). Rotatory power and other optical properties of certain liquid crystals. *Acta Crystallographica, 4*(1), 219–226.
Wang, Q. Q., Zhu, J. Y., Reiner, R. S., Verrill, S. P., Baxa, U., & McNeil, S. E. (2012). Approaching zero cellulose loss in cellulose nanocrystal (CNC) production: recovery and characterization of cellulosic solid residues (CSR) and CNC. *Cellulose, 19*(6), 2033–2047, https://doi.org/10.1007/s10570-012-9765-6.
Wang, R., Chen, L., Zhu, J. Y., & Yang, R. (2017). Tailored and integrated production of carboxylated cellulose nanocrystals (CNC) with nanofibrils (CNF) through maleic acid hydrolysis. *ChemNanoMat, 3*(5), 328–335. https://doi.org/10.1002/cnma.201700015
Zhou, L., Li, N., Shu, J., Liu, Y., Wang, K., Cui, X., et al. (2018). One-pot preparation of carboxylated cellulose nanocrystals and their liquid crystalline behaviors. *ACS Sustainable Chemistry & Engineering, 6*(9), 12403–12410.